

# *NuSTAR* view of the Z-type neutron star low-mass X-ray binary Cygnus X–2

Aditya S. Mondal<sup>1\*</sup>, G. C. Dewangan<sup>2</sup>, M. Pahari<sup>2</sup>, B. Raychaudhuri<sup>1</sup>

<sup>1</sup>Department of physics, Visva-Bharati, Santiniketan, West Bengal-731235, India

<sup>2</sup>Inter-University Centre for Astronomy & Astrophysics (IUCAA), Pune, 411007 India

28 December 2021

## ABSTRACT

We report on the *NuSTAR* observation of the Z-type neutron star low-mass X-ray binary Cygnus X–2 performed on 7 January 2015. During this observation, the source exhibited a sudden decrease in count rate (dips) and stronger variability in 3–79 keV X-ray lightcurve. The hardness-intensity diagram shows that the source remained in the so-called “normal branch” of the Z-track, although an extended “flaring branch” is observed during the dips. The source was in a soft spectral state with the 3–45 keV luminosity of  $L \simeq (0.5 - 1.1) \times 10^{38}$  erg s<sup>−1</sup>, assuming a distance of 8 kpc. Both the non-dip and dip X-ray spectra are well represented by models in which the soft band is dominated by the emission from the disc, while the hard X-ray band is dominated by the Comptonized emission from the boundary layer/corona and its reflected emission from the disc. The X-ray spectrum also revealed a broad Fe K $\alpha$  emission line which is nearly symmetric at the higher flux and asymmetric when the flux is reduced by a factor of  $\sim 2$ . The relativistic reflection model predicts the inner radius of the accretion disc as  $R_{in} \simeq 2.5 - 6.0 R_{ISCO}$  ( $\simeq 30 - 73$  Km) for the non-dip state and  $R_{in} \simeq 2.0 - 2.6 R_{ISCO}$  ( $\simeq 24 - 32$  Km) for the dip state. If the inner disc is truncated due to the pressure arising from a magnetic field, this implies an upper limit of the magnetic field strength of  $\leq 7.6 \times 10^9$  G at the magnetic poles which is consistent with other estimates.

**Key words:** accretion, accretion discs - stars: neutron - X-rays: binaries - stars: individual Cyg X-2

## 1 INTRODUCTION

An X-ray binary consists of a compact star (white dwarf, neutron star or black hole) and a companion star/donor star (may be a main sequence star or an evolved star). If the compact object in an X-ray binary system is a neutron star (NS) and the companion star is a low-mass star ( $\leq 1M_{\odot}$ ), it is called a neutron star low mass X-ray binary (NS LMXB). In NS LMXB systems, the low-mass star loses mass which is accreted onto the weakly magnetized NS. NS LMXBs are usually classified into two sub-classes – the “Z” and “atoll” sources, on the basis of their correlated X-ray spectral and fast timing behavior (Hasinger & van der Klis 1989). Z source traces out a Z-shape pattern in the X-ray colour-colour diagram (CD) on time scales of hours to days. The branches of the Z pattern are called, from top to bottom, the horizontal branch (HB), the normal branch (NB) and the flaring branch (FB). Through the branches, the overall intensity varies smoothly on time scales of weeks

to months. The transition between the HB and the NB is called the hard vertex, and between the NB and the FB the soft vertex. The variations of the mass transfer rate to the compact object are thought to produce the movement along the Z track (e.g. Hasinger & van der Klis 1989; Kuulkers et al. 1996; Wijnands et al. 1997; Lamb 1991). Z sources can further be divided into two groups, the Cyg-like sources (e.g. Cyg X–2, GX 5–1, GX 340+0) and the Sco-like sources (Sco X–1, GX 349+2, GX 17+2). Cyg-like sources display significant motion of their Z pattern in the CD, whereas the Sco-like sources do not. Usually, Cyg-like sources show all three branches of the Z track while for Sco-like sources the HB is weak but FB is much stronger (Church & Bałucińska-Church 2012). Theoretical studies (Psaltis et al. 1995) indicate that the Cyg-like sources are associated with stronger magnetic fields ( $B \sim 5 \times 10^9$  G) than the Sco-like sources ( $B \sim 10^9$  G). Similarly, in Atoll sources the accretion rate increases from the so-called island state to the upper banana branch.

\* E-mail: adityas.mondal@visva-bharati.ac.in

low-mass X-ray binary which is classified as a Z source as it traces out a Z-shape pattern in the X-ray CD (e.g. Hasinger & van der Klis 1989; Kuulkers et al. 1996). It was discovered by Byram et al. (1966) with a sounding rocket experiment. Cyg X-2 was first observed by *EXOSAT* for a continuous time stretch of 14 h starting on July 23, 1984, 02:07 UT with the help of Gas scintillation proportional counter (Peacock et al. 1981) and one half of the medium energy detectors (Turner et al. 1981). The companion of Cyg X-2 is an evolved, late-type star of a mass ranging between  $0.4 - 0.7 M_{\odot}$ , the spectral type of which seems to vary from A5 to F2 (Cowley et al. 1979). The compact object was identified as an NS after the observation of thermonuclear X-ray bursts (Kahn & Grindlay 1984; Smale 1998) in the X-ray lightcurve of Cyg X-2. Titarchuk & Shaposhnikov (2002) used the *RXTE* burst data to estimate the NS mass to be about  $1.4 M_{\odot}$  and the radius to be about 9 km. Moreover, Casares et al. (1998) calculated a neutron star mass of  $1.71 \pm 0.21 M_{\odot}$ , while Elebert et al. (2009) derived a mass of  $1.5 \pm 0.3 M_{\odot}$ . The source itself has an estimated distance of 8 – 11 kpc (Cowley et al. 1979; Smale 1998). Optical observation estimated the source distance to be  $7.2 \pm 1.1$  kpc (Orosz & Kuulkers 1999). Cowley et al. (1979) measured the mass limits of the two components of this binary system and also an orbital period of  $\sim 9.8$  days along with other orbital parameters. Recent high-resolution optical spectroscopy by Casares et al. (2010) also provided a refined orbital solution with a period of  $9.84450 \pm 0.00019$  days. The first 160 days of the *RXTE* (Bradt et al. 1993) All Sky Monitor (ASM) data of Cyg X-2 suggested an 78 day period in the long-term variations (Wijnands et al. 1996). This was also supported by the archival data from *Ariel 5* and *Vela 5B*.

The X-ray spectrum of Cyg X-2 has been studied extensively over the years. The broad band X-ray spectrum of this source has been studied with *BeppoSAX* (Frontera et al. 1999; Di Salvo et al. 2002; Piraino et al. 2002). The spectral analysis using the data from *ASCA* and *BeppoSAX* confirmed the presence of lines from various K-shell ions (Kuulkers et al. 1997; Di Salvo et al. 2002). Like other bright LMXBs, Cyg X-2 also showed the presence of Fe K $\alpha$  emission in its X-ray spectra. H-like Fe xxvi line emission was found by Smale et al. (1993, 1994) using the higher resolution spectrometer of BBXRT. Di Salvo et al. (2002) performed the detailed spectral analysis of the source using the *BeppoSAX* data along the Z-spectral pattern. They fitted the broad band continuum using a two component model, consisting of a disk blackbody and a Comptonized component and detected the broad emission line features at 1 keV and at 6.5 – 6.7 keV. Shaposhnikov et al. (2009) reported the red-skewed iron line profile from the *Suzaku* spectrum of this source. They attributed this as a result of the line formation in the extended wind/outflow configuration instead of the reflection of the X-ray radiation from a cold accretion disk. Done et al. (2002) successfully fitted the *Ginga* data with a reflection model where a Comptonized component irradiates the accretion disk. Cackett et al. (2010) also inferred a broad Fe emission line from the *Suzaku* spectra of Cyg X-2. Many observations of Cyg X-2 indicated an extended accretion disk corona (ADC). Vrtilik et al. (1988)

suggested that high and low flux states reflect changes in the geometrical and optical thickness of the accretion disk and ADC. An evidence of an extended ADC was further supported by the *Chandra* high-resolution grating results (Schulz et al. 2009) on highly excited H-like lines of Ne, Mg, Si, S and Fe in Cyg X-2. The source has been known to exhibit extensive dipping activity in X-ray intensity on the FB. Sometimes hard X-ray tail has been observed in the X-ray spectra of Cyg X-2 (Piraino et al. 2002) which could be due to the presence of a high-energy non-thermal emission.

Accurate timing studies, mainly performed with proportional counter array (PCA) on board the *RXTE* satellite, have shown the presence of rapid variability phenomena such as – quasi-periodic oscillations (QPOs), band limited noise etc. in the frequency range extending from Hz to kHz (Wijnands et al. 1998). Thermonuclear X-ray bursts (Kahn & Grindlay 1984; Smale 1998) have been observed in the X-ray lightcurve of Cyg X-2. Wijnands et al. (1998) reported the simultaneous detection of twin kHz peaks at 500 and 860 Hz and highest single kHz QPO at 1007 Hz. The source exhibited 18 – 50 Hz QPOs in the HB and 5.6 Hz QPOs in the normal branch (Hasinger et al. 1986; Elsner et al. 1986; Wijnands et al. 1997; Kuulkers et al. 1999).

In this paper, we report on the X-ray spectral and timing analysis of high sensitivity, broad bandpass *NuSTAR* observation (Harrison et al. 2013) of Cyg X-2. We particularly focus on the broad relativistic iron line in the  $\sim 5 - 8$  keV band and constrain the stellar radius and/or inner accretion disk radius. In addition, our result confirms the position of the source in the Z-track during this observation. We establish some new results along with reconfirmation of some earlier findings. We organized the paper in the following way. First, we describe the observations and the details of data reduction in sec. 2. In sec. 3 and sec. 4, we describe the temporal and spectral analysis, respectively. In sec. 5, we discuss our findings and we summarize our results in sec. 6.

## 2 OBSERVATION AND DATA REDUCTION

The source Cyg X-2 was observed with *NuSTAR* on 2015 January 7 (MJD 5702.9146) for a total exposure time of  $\sim 23.7$  ks (Obs. ID: 30001141002). *NuSTAR* data were collected with the two co-aligned grazing incidence hard X-ray imaging telescopes (FPMA and FPMB) in the 3 – 79 keV band.

We reprocessed the data using the standard *NuSTAR* data analysis software (*NuSTARDAS* v1.5.1) and *CALDB* (v20150904). We used the *nupipeline* (version v 0.4.3) to filter the event lists. We used a circular region with a radius of 100 arcsec to extract the source events. We also extracted background events from the corner of the detectors devoid of any sources using circular region of similar size as the source region. We employed the task *nuproduct* to create lightcurve, spectra and response files for the FPMA and FPMB. We grouped the FPMA and FPMB spectral data with a minimum of 100 counts per channel, and fitted the two spectra simultaneously.

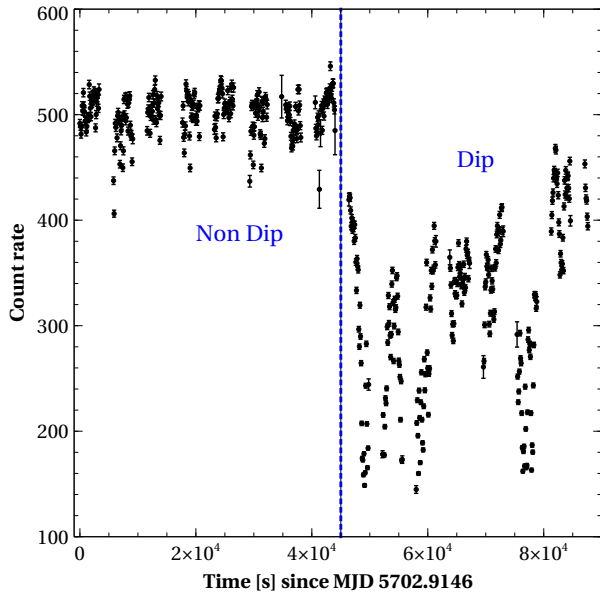


**Figure 1.** The background corrected, full band (3–79 keV) *NuSTAR*/FPMA lightcurve of the source Cyg X-2 with 100 s bins.

### 3 TEMPORAL ANALYSIS

#### 3.1 Light curve

In Fig. 1, we show the 3 – 79 keV *NuSTAR* FPMA light curve of Cyg X-2 spanning  $\sim 1$  day and binned with 100 s. The X-ray lightcurve clearly shows a reduction in intensity from a count rate of  $\sim 500$  counts  $s^{-1}$  in the first half to  $\sim 280$  count  $s^{-1}$  in the second half of the observation. The drop in count rate occurred in  $\sim 5 \times 10^4$  s. In addition, a number of dips in the second half of the observation with decrease in count rates by about a factor of  $\sim 2$  are clearly seen. These variability events appear as absorption dips as observed for many dipping class of LMXBs.

#### 3.2 Hardness ratio and Hardness-intensity diagram

To further investigate the variability of Cyg X-2, we extracted the lightcurves in the 3 – 8 keV and the 8 – 20 keV bands with 100 s bins. These two lightcurves are shown in the upper and middle panel of Fig. 2, respectively. The lower panel of Fig. 2 shows the hardness ratio which is defined as the ratio of counts per second in the 8–20 keV to that in the 3 – 8 keV band. The hardness ratio shows a factor of  $\sim 1.6$  softening of the spectrum during the dips. This behavior is typical and observed for many dipping LMXB sources. The significant hardening in the observed X-ray spectrum indicates a change in the underlying physical conditions.

We further examined the spectral variation of the source by plotting the *NuSTAR* hardness-intensity diagram (HID) which is shown in Fig. 3. We calculated the hardness ratio as the count rate ratio between 9.7 – 16 keV and 6.4 – 9.7 keV while the intensity is defined as the count rate in the 3–16 keV band. We used the same definition of hardness ratio and intensity as that of Wijnands & van der Klis (2001) and Piraino et al. (2002) to compare with the HID of *RXTE*/*BeppoSAX* data. It is seen that the HB

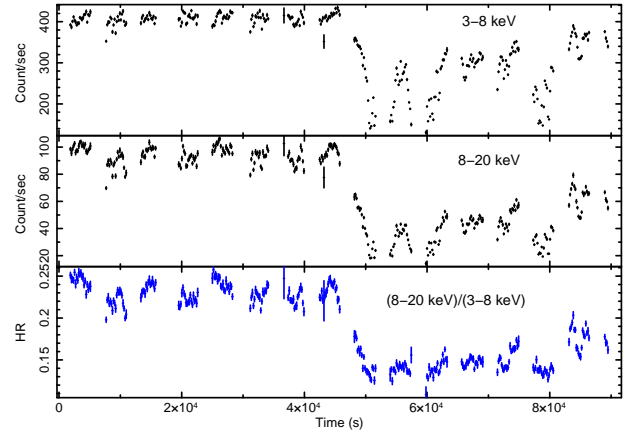


**Figure 2.** The upper and the middle panels show the source count rate in the energy band 3 – 8 keV and 8 – 20 keV, respectively. Bottom panel shows the ratio of count rate in the energy band 8 – 20 keV and 3 – 8 keV.

is not visible in the HID and the source moved along the Normal Branch (NB) of its Z-track. Thus, comparing the HID with earlier work by Piraino et al. (2002) and Wijnands & van der Klis (2001), we confirmed that the source remained in a particular branch, namely the NB, during the *NuSTAR* observation. Although a little deviation from the normal branch has been observed at the lower intensity ( $\sim 200$  counts  $s^{-1}$ ). This might be the transitions between the NB and the FB or an extended FB (according to Wijnands & van der Klis 2001).

#### 3.3 Power density spectra

We extracted power density spectra (PDS) from both the non-dip and the dip part of the *NuSTAR*/FPMA light curve in the energy band 3 – 78 keV. Light curves from both the non-dip and dip part consist of one  $\sim 3$  ks continuous stretch with a bin time of 100 ms. The extracted PDS are rms-normalized and Poisson noise subtracted. PDS from the continuous part of the lightcurve from both the non-dip and dip part are shown in Fig. 4. Here, we observe that at the low frequency (below 0.1 Hz) fractional rms variability during the dip part is higher by few factors than the non-dip part fractional variability. Therefore, long-time scale (10 s or more) variability increases as we move from NB to the extended FB. The increase in fractional rms as we move from the non-dip (NB) to the dip (extended FB) state is consistent with the fact that the higher rms variability at long time scale is expected from the inner disk as it moves closer to the neutron star surface.

### 4 SPECTRAL ANALYSIS

We extracted the FPMA/FPMB spectra after selecting the time intervals and intensities from the *NuSTAR* lightcurve corresponding to non-dip and dip durations (labelled as non-dip and dip in Fig. 1). A non-dip spectrum was selected from the part of the *NuSTAR* lightcurve spanning 0 – 45 ks with intensity  $> 400$  counts  $s^{-1}$ . The dip spectrum was extracted from the interval 46 – 86 ks with intensity  $< 380$  counts

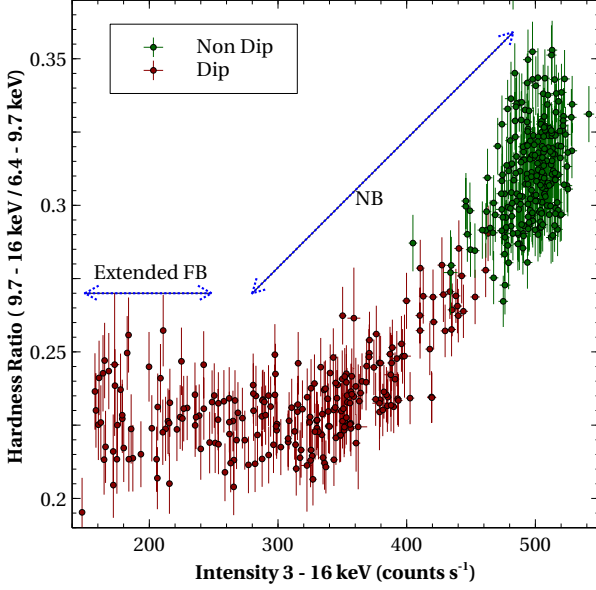


**Figure 3.** The hardness-intensity diagram (HID) of Cyg X-2. Intensity is taken as 3 – 16 keV source count rate and hardness ratio has been taken as the ratio of count rate in the energy band 9.7 – 16 keV and 6.4 – 9.7 keV. The variation of hardness ratio with intensity for the non-dip and dip segments of the lightcurve are shown in green and red colours, respectively.

$\text{s}^{-1}$ . For the non-dip as well as the dip states, we simultaneously fitted *NuSTAR*/FPMA and FPMB spectral datasets using *XSPEC v 12.8.2* (Arnaud 1996). We tied the parameters of the two datasets but introduced a constant factor to account for cross normalization between the two detectors. The constant factor was fixed to 1 for *NuSTAR*/FPMA and kept free for FPMB. We noticed that the source was detected significantly above the background up to  $\simeq 45$  keV. We quote the uncertainties on model parameters at the 90% confidence level.

To begin with, we fitted both the non-dip and dip spectrum separately with a absorbed power-law model. For both the spectra, power-law photon index and the normalization take the values of  $\Gamma \sim 3$  and  $\sim 70 \text{ ph cm}^{-2} \text{ s}^{-1} \text{ keV}^{-1}$ , respectively. We show data to model ratio as a function of energy in Fig. 5. Both the spectra show the presence of some excess in the data to model ratio plot  $\sim 5 - 8$  keV and there may exist a possible cut-off around 10 – 20 keV which are the typical characteristics of the soft state, although no conclusion can be drawn from this plot alone.

#### 4.1 Continuum modeling

We used a continuum spectral model consisting of a soft emission component from the disk (**diskbb** in *XSPEC*) and a thermal Comptonization component **compTT** (Titarchuk 1994), modified by the interstellar absorption modelled by **tbabs** with **vern** cross section (Verner et al. 1996) and **wilm** abundances (Wilms et al. 2000). This two-component model often used by many authors to fit the broadband continuum of many NS LMXBs. The **compTT** model describes the Comptonization of soft photons in a hot plasma (characterised by temperature,  $kT_e$  and optical

depth,  $\tau$ ), and results in spectra with significant curvature close to the plasma temperature. Our continuum model, **tbabs** $\times$ (**diskbb**+**CompTT**), resulted in  $\chi^2/\text{dof}=1523/920$  and 1601/770 for the non-dip and dip spectrum, respectively (where *dof* is the degrees of freedom). The parameters from the continuum spectral fits for the non-dip and the dip spectrum are given in Table 1.

It should be noted that for the Z-track sources, the high energy cut-off is relatively low ( $\sim 5$  keV) which does not allow to determine the powerlaw photon index ( $\Gamma$ ) properly (Bałucińska-Church et al. 2010). In LMXBs the X-ray spectrum above 6 keV or so is typically modelled as either a thermal Comptonization or a hot black body. When we tried to fit the spectra with the combination of a multi-temperature disk black body (**diskbb**) and a single temperature black body (**bbody**) component, an excess of counts above  $\sim 30$  keV was apparent in both the spectra. As the spectra of Z sources sometimes shows the presence of hard tail, we added a power-law component to fit this. This combination of spectral models, **tbabs** $\times$ (**diskbb**+**bbody**+**powerlaw**), is also frequently used for the soft state spectra of many NS LMXBs (Lin et al. 2007; Cackett et al. 2010; Miller et al. 2013). However, such a model does not provide satisfactory fit with  $\chi^2/\text{dof}=1545/920$  and 1650/770 for the non-dip and dip spectra, respectively. The best-fitting continuum parameters for both the spectra are shown in Table 1.

In Fig 6, we show the fitted continuum model **tbabs** $\times$ (**diskbb**+**CompTT**) and the  $\chi$  residuals. Clearly, there are significant residuals near 6 – 7 keV in both spectra and an excess flux in the 12 – 20 keV band which is prominent for the non-dip spectrum compared to the dip spectrum. The broad residuals  $\sim 6 - 7$  keV indicate the presence of a broad iron  $K\alpha$  line. Therefore, we added a **Gaussian** line to model the excess seen  $\sim 6 - 7$  keV. The improvement of the fit was statistically significant with  $\Delta\chi^2 = -452$  and  $-710$  for 3 additional parameters for the non-dip and dip spectrum, respectively. The line is centered at  $\sim 6.44$  keV with a width  $\sigma \sim 0.96$  keV for the non-dip spectrum. For the dip spectrum the width of the line was found to be  $\sigma \sim 0.37$  keV and the center at  $\sim 6.55$  keV. However, **Gaussian** model fails to provide satisfactory fit.

#### 4.2 Reflection Model

Fig. 6 shows clear signature of disk reflection, a broad feature between 5 – 8 keV consistent with Fe  $K\alpha$  emission and a flux excess in the 10 – 20 keV consistent with a Compton back-scattering hump. So, we replaced the **Gaussian** component with a more physical model **reflionx** (Ross & Fabian 2005). Here we used a modified version of the **reflionx**<sup>1</sup> that assumes a black body input spectrum illuminates an accretion disk and produces the reflection spectrum (see e.g. Cackett et al. 2010; King et al. 2016; Degenaar et al. 2016). The parameters of the **reflionx**

<sup>1</sup> [https://www-xray.ast.cam.ac.uk/~mlparker/reflionx\\_models/reflionx\\_alking.mod](https://www-xray.ast.cam.ac.uk/~mlparker/reflionx_models/reflionx_alking.mod)



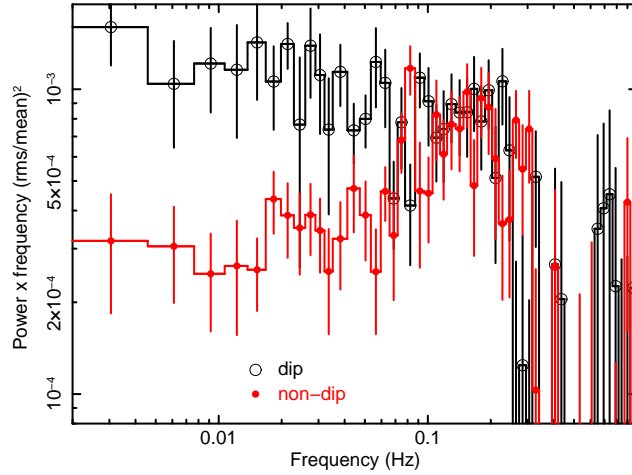


**Figure 4.** PDS obtained after taking 3 ks continuous segments of the non-dip and dip lightcurve using *NuSTAR*/FPMA data in the energy band 3.0 – 78.0 keV with a binning of 100 ms.

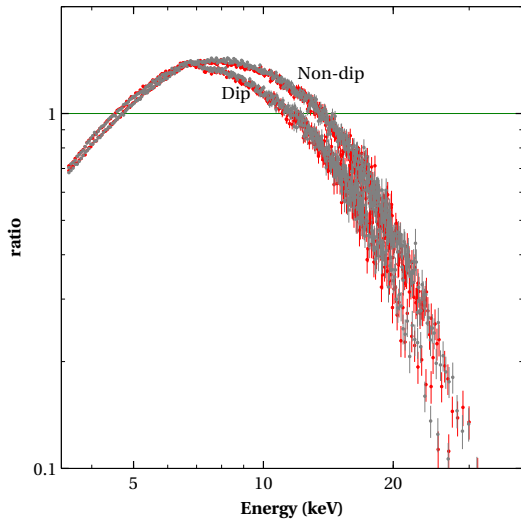


**Figure 5.** Data to model ratio as a function of energy as observed from *NuSTAR* FPMA/FPMB spectra of the source Cyg X-2 in the time interval of non-dip and dip when both the spectra are fitted by an absorbed power-law model.

model are the disc ionization parameter  $\xi$ , the iron abundance  $A_{Fe}$ , the temperature of the ionizing black body flux  $kT_{refl}$  and a normalization  $N_{refl}$ . In order to account the relativistic effects, we used the convolution kernel **relconv** (Dauser et al. 2010). In this model, the emissivity of the disk is described as a broken powerlaw in radius (e.g.,  $\epsilon \propto r^{-q}$ ), giving three parameters:  $q_{in}$ ,  $q_{out}$  and  $R_{break}$ . Here we used an unbroken emissivity profile (fixed slope) by fixing  $q_{out} = q_{in}$  (obviating the meaning of  $R_{break}$ ) as the slope is not constrained by the data. The parameters of the **relconv** model are the emissivity index  $q$ , the inner and outer disk radius  $R_{in}$  and  $R_{out}$ , the disk inclination  $i$  and the dimensionless spin parameter  $a$ . We set the emissivity to  $q = 3$ , in agreement with a Newtonian geometry far from the NS (Cackett et al. 2010). The spin frequency of the source Cyg X-2 can be taken as  $\sim 364$  Hz (Wijnands et al. 1998). Following Braje et al. (2000), the dimensionless spin

**Table 1.** Parameters of the continuum models for the non-dip and the dip spectrum.  $1\sigma$  error on all relevant parameters are quoted.

Model:TBabs $\times$ (diskbb+compTT)		
Parameter	Non Dip	Dip
$kT_{in}$ ( keV )	$1.57^{+0.08}_{-0.19}$	$1.28^{+0.06}_{-0.12}$
$kT_e$ ( keV )	$4.45^{+7.84}_{-0.70}$	$2.42^{+0.11}_{-0.04}$
$kT_{seed}$ ( keV )	$2.03^{+0.23}_{-0.32}$	$1.11^{+0.05}_{-0.09}$
$\tau$	$1.90^{+0.74}_{-1.45}$	$5.47^{+1.00}_{-1.20}$
Model:TBabs $\times$ (diskbb+bbbody+powerlaw)		
$kT_{in}$ ( keV )	$1.76 \pm 0.01$	$1.42 \pm 0.01$
$kT_{bb}$ ( keV )	$2.63 \pm 0.05$	$2.26 \pm 0.04$
$\Gamma$	$3.41 \pm 0.12$	$2.05^{+1.39}_{-1.70}$

Note:  $kT_{in}$ = inner disk temperature,  $kT_e$ = electron temperature of the Comptonizing plasma,  $kT_{seed}$ = seed photon temperature and  $kT_{bb}$ = blackbody temperature.

parameter  $a$  can be approximated as  $a \simeq 0.47/P_{ms}$  where  $P_{ms}$  is the spin period in ms. Therefore, we fixed the spin parameter to  $a = 0.17$ . We also fixed the outer radius  $R_{out} = 1000 R_G$ .

The addition of the relativistic reflection model improved the spectral fits significantly ( $\chi^2/dof=1037/914$  and  $\chi^2/dof=873/765$  for the non-dip and dip spectrum, respectively). The best-fit parameters are shown in Table 2. The best-fit inner disk radius lies at  $R_{in} = (2.5 - 6.0)R_{ISCO}$  for non-dip state and  $R_{in} = (2.0 - 2.6)R_{ISCO}$  for the dip state. The inclination angle is found to be  $i = 23 \pm 2$  degree (consistent with Cackett et al. 2010). The reflection component

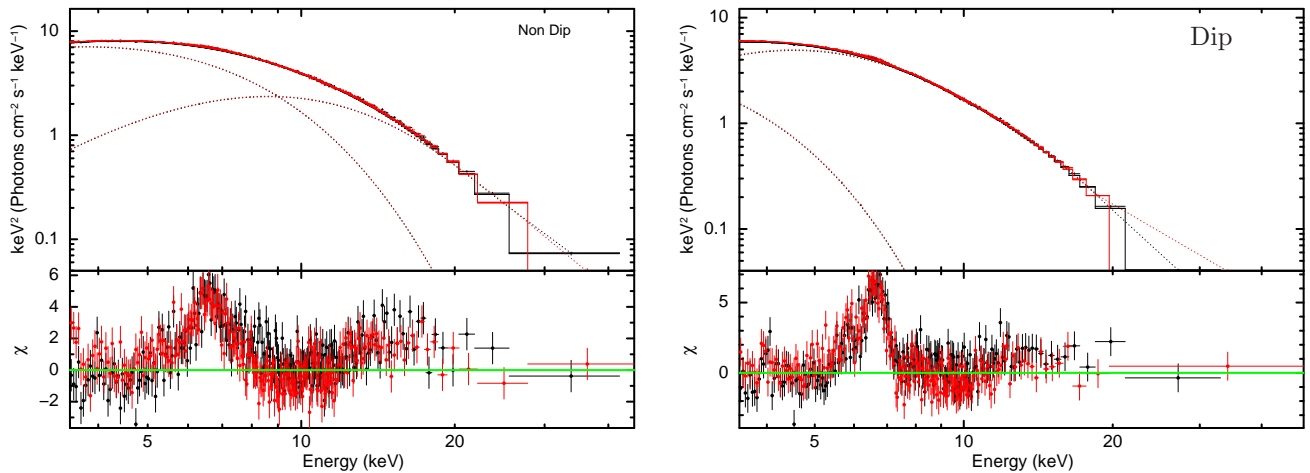


**Figure 6.** *NuSTAR* (FPMA in black, FPMB in red) unfolded spectra. The spectral data were rebinned for visual clarity. Continuum is fitted with the model consisting of a disk blackbody and Comptonized emission. Model used: `TBabs*(diskbb+compTT)`. It revealed un-modelled broad emission line  $\sim 6 - 7$  keV as well as the higher energies.

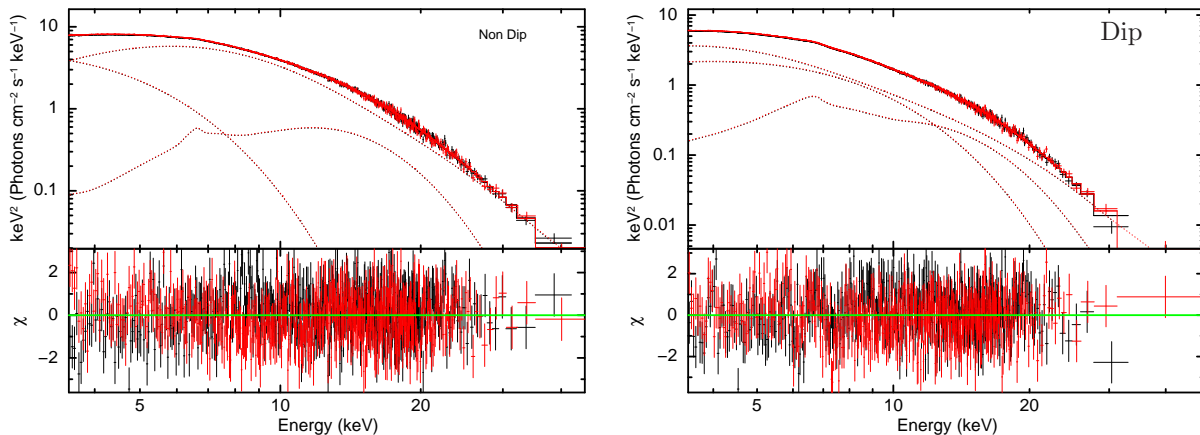


**Figure 7.** The *NuSTAR* (FPMA in black, FPMB in red) unfolded spectra of Cyg X-2 in the non-dip (left) and dip states (right) and the best-fitting fitted model consisting of a disk blackbody, Comptonized emission and relativistically blurred reflection i.e., `TBabs*(diskbb+compTT+relconv*reflionx)`. Lower panel shows residuals in units of  $\sigma$ .

has an intermediate disc ionization of  $\xi \simeq 70 - 400 \text{ erg s}^{-1} \text{ cm}$  which is the typical range observed in both black hole and NS LMXBs ( $\log \xi \sim 2 - 3$ ). The Fe abundance is less than that of solar composition ( $\leq 0.7$ ) for the non-dip spectrum and for the dip spectrum it was frozen to the value obtained from the non-dip spectrum as it was not well constrained. The fitted spectra (both non-dip and dip) along with the model components and the residuals are shown in Fig. 7.

## 5 DISCUSSION

We report on the *NuSTAR* observation of the bright Z-type low mass X-ray binary Cyg X-2. From the hardness-intensity diagram (HID), it is confirmed that the source was in the so-called NB on the Z-track during this observation, although an extended FB is observed when the source move from non-dip to dip state. An increase in the fractional rms has been observed from the PDS as the source move from non-dip (NB) to dip (extended FB) state. Higher

rms variability at long time scale is expected from the inner disc which moves closer to the NS surface. This is consistent with results from spectral analysis which show that as the source moves from non-dip to dip part, the inner disk radius decreases and the disk temperature increases. The broad-band  $3 - 45 \text{ keV}$  *NuSTAR* spectral data can be described by a continuum model consisting of a disk blackbody and thermal Comptonization. The source was in a soft spectral state with the  $3 - 45 \text{ keV}$  luminosity of  $L \simeq (0.5 - 1.1) \times 10^{38} \text{ ergs s}^{-1}$ , assuming a distance of 8 kpc. The spectral data required a significant reflection component, characterised by the broad Fe  $K\alpha$  emission line.

From Fig. 6, it has been observed that there are differences between the Fe line profiles from non-dip and dip spectrum. During non-dip state, the Fe line profile is symmetric and there is a hump like structure at  $15 - 30 \text{ keV}$ . While during dip state, Fe line profile is mostly asymmetric and  $15 - 30 \text{ keV}$  hump is significantly reduced. Symmetric line profile essentially indicate the existence of strong

**Table 2.** Best-fit non-dip and dip spectral parameters of the *NuSTAR* observation of the source Cyg X-2 using model: TBabs $\times$ (diskbb+compTT+relconv\*reflionx).  $1\sigma$  error on all relevant parameters are quoted.

Component	Parameter	NuSTAR spectrum	
		Non Dip	Dip
TBABS	$N_H (\times 10^{22} \text{ cm}^{-2})$	0.22( <i>f</i> )	0.22( <i>f</i> )
DISKBB	$kT_{in}$ (keV)	$0.99^{+0.18}_{-0.10}$	$1.66 \pm 0.05$
	$N_{diskbb} [(\text{km}/10 \text{ kpc})^2 \cos i]$	$735^{+223}_{-321}$	$45^{+10}_{-8}$
COMPTT	$kT_{seed}$ (keV)	$1.33 \pm 0.05$	$0.76 \pm 0.01$
	$kT_e$ (keV)	$5.97^{+7.25}_{-1.42}$	$3.78^{+1.61}_{-0.68}$
	$\tau$	$1.03^{+0.40}_{-0.44}$	$2.09^{+0.93}_{-1.01}$
	$n_{comptt}^a$	$0.16 \pm 0.14$	$0.60^{+0.19}_{-0.24}$
RELCONV	$i$ (degrees)	$\leq 21$	$23 \pm 2$
	$R_{in} (\times R_{ISCO})$	$4.3 \pm 1.8$	$2.0^{+0.52}_{-0.26}$
REFLIONX	$\xi (\text{erg cm s}^{-1})$	$69^{+30}_{-10}$	$390^{+80}_{-130}$
	$A_{Fe} (\times \text{Solar})$	$0.5^{+0.16}_{-0.4}$	0.7( <i>f</i> )
	$kT_{refl}$ (keV)	$2.45^{+0.10}_{-0.07}$	$2.20 \pm 0.09$
	$N_{refl}^b$	$11.6^{+2.2}_{-4.2}$	$2.4^{+0.30}_{-0.16}$
	$F_{total}^* (\times 10^{-8} \text{ ergs/s/cm}^2)$	$1.58 \pm 0.01$	$0.95 \pm 0.01$
	$F_{diskbb} (\times 10^{-8} \text{ ergs/s/cm}^2)$	$0.39 \pm 0.01$	$0.35 \pm 0.01$
	$F_{comptt} (\times 10^{-8} \text{ ergs/s/cm}^2)$	$1.07 \pm 0.01$	$0.51 \pm 0.01$
	$F_{reflionx} (\times 10^{-8} \text{ ergs/s/cm}^2)$	$0.12 \pm 0.01$	$0.09 \pm 0.01$
	$L_{3-79 \text{ keV}} (\times 10^{38} \text{ ergs/s})$	$1.21 \pm 0.01$	$0.73 \pm 0.01$
	$\chi^2/dof$	1037/914	873/765

The outer radius of the **relconv** spectral component was fixed to  $1000 R_G$  and the spin parameter was set to  $a = 0.17$  and  $q = 3$ . <sup>a,b</sup> denotes the normalization component of the **compTT** and **relconv** model, respectively. Assumed a distance of 8 kpc and a mass of  $1.5 M_\odot$  for calculating the luminosity. \*All the fluxes are calculated in the energy band 3.0 – 79.0 keV.

outflow/wind in the system which causes broadening of the blue wing of the line. However, such outflow is not present during dip state and we get an asymmetric line profile due to redshift only. Such scenario is further supported by the enhanced Comptonized flux during non-dip state ( $\sim 20\%$  or so). Comptonization may occur also from the outflow and therefore it is increased during non-dip state. The enhanced Comptonization due to the presence of outflow/wind can provide stronger Compton back-scattering hump which is clearly visible in non-dip spectrum but faint in dip spectrum because of the absence of outflow/wind. The change in the shape of the HID is possibly due to the change in outflow properties (like wind on and off) which may affects the accretion geometry. This might be

responsible for different seed photon temperature ( $kT_{seed}$ ) in the non-dip and dip state for Comptonization. During this observation, a decrease in the hardness ratio (a factor of  $\sim 1.6$  or so) has been observed when the source passes from the non-dip to the dip states. So, there is a softening of the spectrum during the dip state. This indicate that the transition from non-dip state to dip state is unlikely to be due to the absorption. From the final best-fit model, we found that the **diskbb** component became more dominant from non-dip to dip state ( $\sim 15\%$  increment in the **diskbb** flux), while the comptonization component became weaker with decreasing cutoff energy, indicating a decrease in  $kT_e$ . The optical depth,  $\tau$ , is higher in the dip state compared to

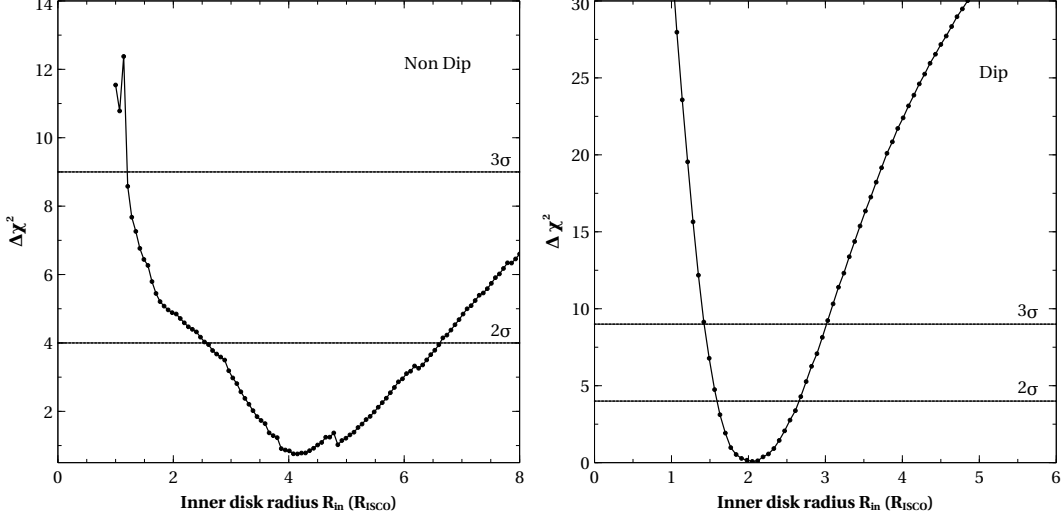


**Figure 8.** Both the panels shows the variation of  $\Delta\chi^2 (= \chi^2 - \chi^2_{min})$  as a function of inner disc radius (in the unit of  $R_{ISCO}$ ) obtained from the relativistic reflection model. We varied the inner disc radius as a free parameter upto  $8 R_{ISCO}$ . Horizontal lines in both the panels indicate  $2\sigma$  and  $3\sigma$  significance level.

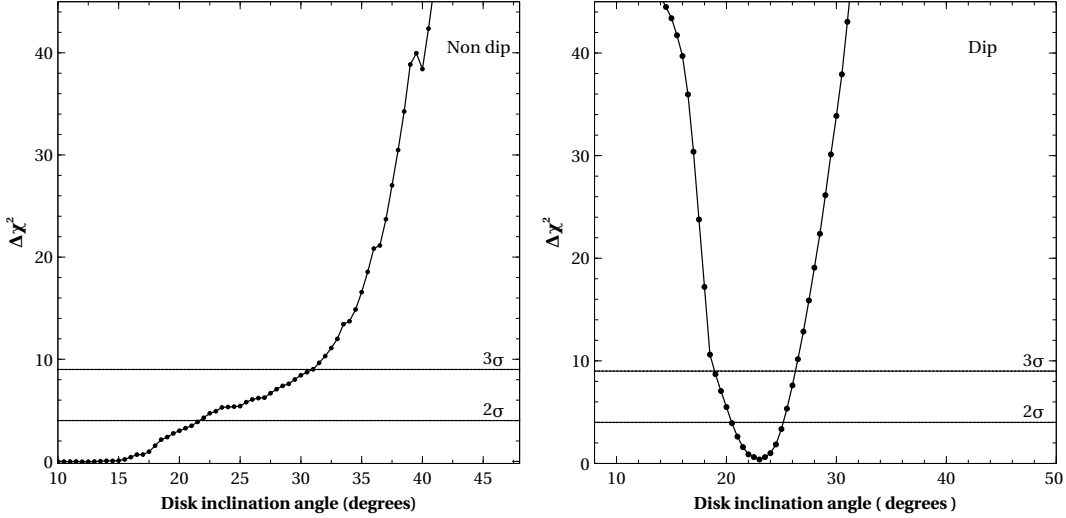


**Figure 9.** Disk inclination angle delta chi-squared ( $\Delta\chi^2$ ) distribution in the relativistic reflection model. We varied the disc inclination angle between 10 degree and 50 degree in both the states. Horizontal lines in both the panels indicate  $2\sigma$  and  $3\sigma$  significance level

the non-dip state.

We fitted the reflection features with a relativistically blurred reflection model. We found that the line has an intermediate disc ionization ( $\xi \sim 70 - 400 \text{ erg s}^{-1} \text{ cm}$ ) and a relatively low viewing angle ( $i \sim 23 \text{ deg}$ ) but a large inner radius ( $R_{in} = 2.5 - 6.0 \times R_{ISCO}$  from the non-dip spectrum and  $R_{in} = 2.0 - 2.6 \times R_{ISCO}$  from the dip spectrum). Following van der Klis (2000),  $R_{ISCO}$  can be approximated as  $R_{ISCO} \simeq (6GM/c^2)(1 - 0.54a)$ . Thus for the spin parameter  $a = 0.17$  and  $1.5 M_{\odot}$  NS  $R_{ISCO} = 5.4 GM/c^2$ . So, the inner disk radius was located far from the NS surface at  $R_{in} \simeq 13.5 - 32.4 GM/c^2$  ( $\simeq 30 - 73 \text{ km}$ ), estimated from non-dip spectrum and at  $R_{in} \simeq 10.8 - 14 GM/c^2$  ( $\simeq 24 - 32 \text{ km}$ ) estimated from dip spectrum. Larger inner disk radius was also obtained by Done et al. (2002) after fitting *Ginga*

data with the reflection model.

We compared the inner disk radius from the Fe line fitting with that implied from the `diskbb` fits. The normalization component of the `diskbb` is defined as  $N_{diskbb} = (R_{in,diskbb}/D_{10})^2 \cos i$  (where  $R_{in,diskbb}$  in km and  $D_{10}$  is the distance in units of 10 kpc), which can be used as an important probe to constrain the inner radial extent of the accretion disk. Although the large uncertainties involving in factors like inner boundary assumptions (Gierliński et al. 1999), spectral hardening (Merloni et al. 2000), the column density or inclination etc. hamper the measurement of the true inner-disk radii from `diskbb` fits. From our best fit `diskbb` normalization, we obtained an inner disk radius of  $R_{in,diskbb} \simeq 17 - 26 \text{ km}$  from the non-dip spectrum and  $R_{in,diskbb} \simeq 7 - 9 \text{ km}$  from the dip spectrum



for an inclination of  $i = 21 - 25$  deg and distance of 8 kpc. However, if we corrected it with the hardening factor  $\simeq 1.7$  (e.g. Kubota et al. 2001; Reynolds & Miller 2013), then it yielded  $R_{in,diskbb} \simeq 49 - 74$  km from the non-dip spectrum and  $R_{in,diskbb} \simeq 20 - 26$  km from the dip spectrum those are consistent with the location of the inner disk inferred from the reflection model in both spectra. In General, NS LMXBs exhibit a wide range of inferred inner disc radii, most sources show small inner disk radii of  $6 - 15 GM/c^2$  (see Cackett et al. 2010; Degenaar et al. 2015; Di Salvo et al. 2015), some sources show slightly larger inner radius of  $15 - 30 GM/c^2$  (see Iaria et al. 2016; Miller et al. 2011; Papitto et al. 2013; King et al. 2016). At the same time, a significantly larger truncation radii of  $\geq 80 GM/c^2$  has been observed for two NS LMXBs (Degenaar et al. 2016, 2014). In this observation of the source Cyg X-2, we have observed a moderate disc truncation of inner disc radii  $\simeq 11 - 32 GM/c^2$ . If it is assumed that the truncation of the disc is caused by the magnetosphere, it would imply a large NS magnetic field ( $\geq 4 \times 10^8$  G).

We can assume that the inner accretion disk is truncated at the magnetospheric radius rather than its surface. At the magnetospheric radius, magnetic pressure balances the ram pressure from the infalling material. From the source luminosity and reasonable assumption about mass and radius, we can estimate the magnetic field strength. We used the following equation of Cackett et al. (2009) which was a modified version of the formulation of Ibragimov & Poutanen (2009) to calculate the magnetic dipole moment.

$$\mu = 3.5 \times 10^{23} k_A^{-7/4} x^{7/4} \left( \frac{M}{1.4 M_\odot} \right)^2 \times \left( \frac{f_{ang}}{\eta} \frac{F_{bol}}{10^{-9} \text{ erg cm}^{-2} \text{ s}^{-1}} \right)^{1/2} \frac{D}{3.5 \text{ kpc}} \text{ G cm}^3 \quad (1)$$

where  $\eta$  is the accretion efficiency in the Schwarzschild metric,  $f_{ang}$  is the anisotropy correction factor. The coefficient  $k_A$  depends on the conversion from spherical to disk accretion (numerical simulation suggest  $k_A = 0.5$  whereas theoretical model predict  $k_A < 1.1$ ). Cackett et al. (2009) modified  $R_{in}$  as  $R_{in} = x GM/c^2$ . We estimated flux in the  $0.01 - 100$  keV range is of  $F_{bol} = 2.2 \times 10^{-8} \text{ erg cm}^{-2} \text{ s}^{-1}$ . We assumed  $D = 8$  kpc,  $M = 1.5 M_\odot$  and  $R = 10$  km. Using  $R_{in} \leq 32 R_G$  from the *NuSTAR* Fe line fit, along with assuming  $k_A = 1$ ,  $f_{ang} = 1$  and  $\eta = 0.1$ , leads to magnetic field strength of  $B \leq 7.6 \times 10^9$  G at the magnetic poles. This value is consistent with Wijnands et al. 1996 ( $\sim 8.5 \times 10^9$  G) when the source enters in the normal branch of the Z track. However, if we assume  $k_A = 0.5$ , the magnetic field strength is increased nearly by a factor of 3.

We calculated the Keplerian frequency associated with the truncation radius using the following relation by van der Klis (2000)

$$\nu_{orb} \approx 1200 (r_{orb}/15 \text{ km})^{-3/2} m_{1.4}^{1/2} \text{ Hz} \quad (2)$$

which was found to be in the range  $155 - 611$  Hz. This frequency range is consistent with the spin frequency of Cyg X-2 if the difference between kHz QPO of  $\sim 364$  Hz is

taken as a spin estimate (Wijnands et al. 1998).

## 6 SUMMARY

In this paper, we have analyzed a *NuSTAR* observation of the Z-type NS LMXB Cyg X-2. Our findings obtained from the timing and the spectral studies may be summarized as follows –

- The source exhibited a sudden decrease in the count rate (dips) and stronger variability in  $3 - 79$  keV lightcurve.
- It is confirmed from the HID that the source was in the so-called NB on the Z-track during this observation, although an extended FB is observed when the source moves from non-dip to dip state.
- An increase in the fractional rms has been observed from the PDS as the source move from the non-dip (NB) to the dip (extended FB) state.
- The broad band  $3 - 45$  keV *NuSTAR* spectral data can be described by a continuum model consisting of a disk blackbody and thermal Comptonization.
- The source was found in a soft spectral state with the  $3 - 45$  keV luminosity of  $L \simeq (0.5 - 1.1) \times 10^{38} \text{ ergs s}^{-1}$ , assuming a distance of 8 Kpc.
- We found broad, relativistic Fe  $K\alpha$  emission line and a hump like structure at  $15 - 30$  keV. From the relativistic reflection model fitting, we were able to measure the inner radius of the accretion disc.
- The Keplerian frequency associated with the truncation radius was found to be in the range  $155 - 611$  Hz.
- We estimated an upper limit of the magnetic field strength of  $\leq 7.6 \times 10^9$  G at the magnetic poles with an assumption that the disc is truncated at the magnetospheric radius.

## 7 ACKNOWLEDGEMENTS

This research has made use of data and/or software provided by the High Energy Astrophysics Science Archive Research Centre (HEASARC). Aditya S. Mondal would like to thank Inter-University Centre for Astronomy and Astrophysics (IUCAA), Pune, India for hosting him during his visits. BR likes to thank IUCAA for hospitality and other facilities extended to him during his visits under the Visiting Associateship programme.

## REFERENCES

- Arnaud K. A., 1996, in *Astronomical Society of the Pacific Conference Series*, Vol. 101, *Astronomical Data Analysis Software and Systems V*, Jacoby G. H., Barnes J., eds., p. 17
- Bałucińska-Church M., Gibiec A., Jackson N. K., Church M. J., 2010, *A&A*, 512, A9
- Bradt H. V., Rothschild R. E., Swank J. H., 1993, *A&AS*, 97, 355
- Braje T. M., Romani R. W., Rauch K. P., 2000, *ApJ*, 531, 447
- Byram E. T., Chubb T. A., Friedman H., 1966, *AJ*, 71, 379

- Cackett E. M., Altamirano D., Patruno A., Miller J. M., Reynolds M., Linares M., Wijnands R., 2009, *ApJ*, 694, L21
- Cackett E. M. et al., 2010, *ApJ*, 720, 205
- Casares J., Charles P., Kuulkers E., 1998, *ApJ*, 493, L39
- Casares J., González Hernández J. I., Israelian G., Rebolo R., 2010, *MNRAS*, 401, 2517
- Church M. J., Bałucińska-Church M., 2012, *MmSAI*, 83, 170
- Cowley A. P., Crampton D., Hutchings J. B., 1979, *ApJ*, 231, 539
- Dauser T., Wilms J., Reynolds C. S., Brenneman L. W., 2010, *MNRAS*, 409, 1534
- Degenaar N., Koljonen K. I. I., Chakrabarty D., Kara E., Altamirano D., Miller J. M., Fabian A. C., 2016, *MNRAS*, 456, 4256
- Degenaar N., Miller J. M., Chakrabarty D., Harrison F. A., Kara E., Fabian A. C., 2015, *MNRAS*, 451, L85
- Degenaar N., Miller J. M., Harrison F. A., Kennea J. A., Kouveliotou C., Younes G., 2014, *ApJ*, 796, L9
- Di Salvo T. et al., 2002, *A&A*, 386, 535
- Di Salvo T. et al., 2015, *MNRAS*, 449, 2794
- Done C., Życki P. T., Smith D. A., 2002, *MNRAS*, 331, 453
- Elebert P., Callanan P. J., Torres M. A. P., Garcia M. R., 2009, *MNRAS*, 395, 2029
- Elsner R. F., Weisskopf M. C., Darbro W., Ramsey B. D., Williams A. C., Sutherland P. G., Grindlay J. E., 1986, *ApJ*, 308, 655
- Frontera F. et al., 1999, *A&AS*, 138, 399
- Gierliński M., Zdziarski A. A., Poutanen J., Coppi P. S., Ebisawa K., Johnson W. N., 1999, *MNRAS*, 309, 496
- Harrison F. A. et al., 2013, *ApJ*, 770, 103
- Hasinger G., Langmeier A., Sztajno M., Truemper J., Lewin W. H. G., 1986, *Nature*, 319, 469
- Hasinger G., van der Klis M., 1989, *A&A*, 225, 79
- Iaria R. et al., 2016, *A&A*, 596, A21
- Ibragimov A., Poutanen J., 2009, *MNRAS*, 400, 492
- Kahn S. M., Grindlay J. E., 1984, *ApJ*, 281, 826
- King A. L. et al., 2016, *ApJ*, 819, L29
- Kubota A., Mizuno T., Makishima K., Fukazawa Y., Kotoku J., Ohnishi T., Tashiro M., 2001, *ApJ*, 547, L119
- Kuulkers E., Parmar A. N., Owens A., Oosterbroek T., Lammers U., 1997, *A&A*, 323, L29
- Kuulkers E., van der Klis M., Vaughan B. A., 1996, *A&A*, 311, 197
- Kuulkers E., Wijnands R., van der Klis M., 1999, *MNRAS*, 308, 485
- Lamb F. K., 1991, in *Astronomical Society of the Pacific Conference Series*, Vol. 20, *Frontiers of Stellar Evolution*, Lambert D. L., ed., pp. 299–388
- Lin D., Remillard R. A., Homan J., 2007, *ApJ*, 667, 1073
- Merloni A., Fabian A. C., Ross R. R., 2000, *MNRAS*, 313, 193
- Miller J. M., Maitra D., Cackett E. M., Bhattacharyya S., Strohmayer T. E., 2011, *ApJ*, 731, L7
- Miller J. M. et al., 2013, *ApJ*, 779, L2
- Orosz J. A., Kuulkers E., 1999, *MNRAS*, 305, 132
- Papitto A. et al., 2013, *MNRAS*, 429, 3411
- Peacock A., Andresen R. D., Manzo G., Taylor B. G., Villa G., Re S., Ives J. C., Kellock S., 1981, *SSRv*, 30, 525
- Piraino S., Santangelo A., Kaaret P., 2002, *ApJ*, 567, 1091
- Psaltis D., Lamb F. K., Miller G. S., 1995, *ApJ*, 454, L137
- Reynolds M. T., Miller J. M., 2013, *ApJ*, 769, 16
- Ross R. R., Fabian A. C., 2005, *MNRAS*, 358, 211
- Schulz N. S., Huenemoerder D. P., Ji L., Nowak M., Yao Y., Canizares C. R., 2009, *ApJ*, 692, L80
- Shaposhnikov N., Titarchuk L., Laurent P., 2009, *ApJ*, 699, 1223
- Smale A. P., 1998, *ApJ*, 498, L141
- Smale A. P., Angelini L., White N. E., Mitsuda K., Dotani T., 1994, in *Bulletin of the American Astronomical Society*, Vol. 26, *American Astronomical Society Meeting Abstracts*, p. 1484
- Smale A. P. et al., 1993, *ApJ*, 410, 796
- Titarchuk L., 1994, *ApJ*, 434, 570
- Titarchuk L., Shaposhnikov N., 2002, *ApJ*, 570, L25
- Turner M. J. L., Smith A., Zimmermann H. U., 1981, *SSRv*, 30, 513
- van der Klis M., 2000, in *Rossi2000: Astrophysics with the Rossi X-ray Timing Explorer*, Strohmayer T. E., ed.
- Verner D. A., Ferland G. J., Korista K. T., Yakovlev D. G., 1996, *ApJ*, 465, 487
- Vrtilek S. D., Swank J. H., Kelley R. L., Kahn S. M., 1988, *ApJ*, 329, 276
- Wijnands R. et al., 1998, *ApJ*, 493, L87
- Wijnands R., van der Klis M., 2001, *MNRAS*, 321, 537
- Wijnands R. A. D., Kuulkers E., Smale A. P., 1996, *ApJ*, 473, L45
- Wijnands R. A. D., van der Klis M., Kuulkers E., Asai K., Hasinger G., 1997, *A&A*, 323, 399
- Wilms J., Allen A., McCray R., 2000, *ApJ*, 542, 914